Ultrafast and sensitive photodetector based on a PtSe$_2$/silicon nanowire array heterojunction with a multiband spectral response from 200 to 1550 nm

Longhui Zeng[1], Shenghuang Lin[1], Zhenhua Lou[2], Huiyu Yuan [1], Hui Long[1], Yanyong Li[1], Wei Lu[1], Shu Ping Lau [1], Di Wu[2] and Yuen Hong Tsang[1,3]

Abstract

The newly discovered Group-10 transition metal dichalcogenides (TMDs) like PtSe$_2$ have promising applications in high-performance microelectronic and optoelectronic devices due to their high carrier mobilities, widely tunable bandages and ultrastabilities. However, the optoelectronic performance of broadband PtSe$_2$ photodetectors integrated with silicon remains undiscovered. Here, we report the successful preparation of large-scale, uniform and vertically grown PtSe$_2$ films by simple selenization method for the design of a PtSe$_2$/Si nanowire array heterostructure, which exhibited a very good photoresponsivity of 12.65 A/W, a high specific detectivity of 2.5×10^{13} Jones at −5 V and fast rise/fall times of 10.1/19.5 μs at 10 kHz without degradation while being capable of responding to high frequencies of up to 120 kHz. Our work has demonstrated the compatibility of PtSe$_2$ with the existing silicon technology and ultrabroad band detection ranging from deep ultraviolet to optical telecommunication wavelengths, which can largely cover the limitations of silicon detectors. Further investigation of the device revealed pronounced photovoltaic behavior at 0 V, making it capable of operating as a self-powered photodetector. Overall, this representative PtSe$_2$/Si nanowire array-based photodetector offers great potential for applications in next-generation optoelectronic and electronic devices.

Introduction

Photodetectors (PDs), one of the most important types of optoelectronic devices, can covert incident light into an electrical signal[1]. They have received considerable research interest, as this technology is essential for a variety of industrial and scientific applications and has a large impact on our daily lives. These applications include imaging, optical telecommunication, remote control technologies, day- and night-time surveillance and environmental monitoring[2–4]. In comparison to narrowband PDs, broadband PDs can meet the demands of ultraviolet–visible–infrared light communication, wide spectral switches or memory storage by using only a single device. To date, significant efforts have been focused on the development of broadband PDs based on quantum dots[5], inorganic nanomembranes[6] and organic perovskite[7], but these developed devices are still limited by a slow response speed and relatively short detection range. To date, a challenge still remains for simultaneously achieving a faster response speed and broader detection range by exploring new materials. For example, the

Correspondence: Di Wu (wudi1205@zzu.edu.cn) or Yuen Hong. Tsang (yuen.tsang@polyu.edu.hk)
[1]Department of Applied Physics and Materials Research Center and University Research Facility in Materials Characterization and Device Fabrication, The Hong Kong Polytechnic University, Hung Hom, Kowloon, Hong Kong 99077, China
[2]Department of Physics and Engineering, and Key Laboratory of Material Physics, Zhengzhou University, Zhengzhou, Henan 450052, People's Republic of China
Full list of author information is available at the end of the article
These authors contributed equally: Longhui Zeng, Shenghuang Lin.

traditional silicon has been a common and excellent material of choice for commercial PDs owing to its low cost and well-developed fabrication processes for large-area detectors[8]. Compared with their thin film counterparts, vertically standing silicon nanowire array (SiNWA) structures can strongly suppress light reflection, increase the interfacial area, facilitate fast charge transport and enhance charge collection by shortening the travel paths of minority carriers[9,10]. However, the spectral response of Si-based PDs is limited by the natural bandgap (~1.12 eV), corresponding to a range of 400–1100 nm[6,11]. To develop Si-based PDs with a broadband response, heterostructures with various designs have been suggested, including a heterojunction between Si and an organic semiconductor for extending photodetection to the ultraviolet (UV) region[12], and heterogeneous integration of Si with Ge to provide sensitivity to the infrared (IR) region[13]. However, the instability and poor performance of these heterostructures limit their practical applications.

Recently, the increasingly popular two-dimensional (2D) materials have become of great interest for application in future micro- and nano-optoelectronics owing to their outstanding electronic, optical and mechanical properties[14–17]. In particular, the newly discovered PtSe₂, a promising member of the Group-10 transition metal dichalcogenides (TMDs), has been theoretically predicted to have a high carrier mobility and tunable bandgap ranging from 1.2 eV (monolayer) to 0.21 eV (bilayer) at room temperature. However, the multilayer 1T-phase PtSe₂ exhibits a broad light absorption spectrum because of its semi-metallic character[18,19]. The current approaches for fabricating PtSe₂ layers are limited to mechanical exfoliation[19] and chemical vapor deposition[20], which usually yield PtSe₂ nanosheets with uncontrollable sizes. Another approach to obtaining single-crystalline PtSe₂ and a large film of layered PtSe₂ is molecular beam epitaxy, but this method suffers from a high cost and slow growth rate[18,21]. Recently, scalable and horizontal 2D layered PtSe₂ films prepared by either an aqueous-phase reaction[22] or thermally assisted conversion[23,24] are considered as prerequisites for electronic and optoelectronic device applications. For example, Yim et al.[24] reported that vertically stacked heterostructures were successfully realized by directly transferring PtSe₂ films onto a Si substrate, resulting in enhanced photoelectrical properties such as rectifying and photovoltaic behaviors. However, comprehensive investigations of PtSe₂-based photodetectors and their key parameters, including the spectral selectivity, response speed and specific detectivity, have not yet been conducted.

Here, wafer-scale, high-quality and continuous 2D PtSe₂ films with vertically standing layered structures were successfully synthesized via selenization of sputtered Pt films, which paves the way for obtaining high-growth-rate wafer-scale films with precise thickness control. The obtained vertical PtSe₂ films were then transferred to an *n*-type SiNWA to form broadband photodetectors. The light absorption of the PtSe₂ film was enhanced by an increase in the film thickness, whereas the vertically standing layered structure greatly facilitated the transport of photogenerated carriers along the in-plane direction to the top electrode[25]. Significantly, the PDs revealed a multiband detection range (200–1550 nm) and fast response time (10.1/19.5 µs). Our study demonstrated the feasibility of utilizing these proposed materials for future high-speed and broadband optoelectronic devices.
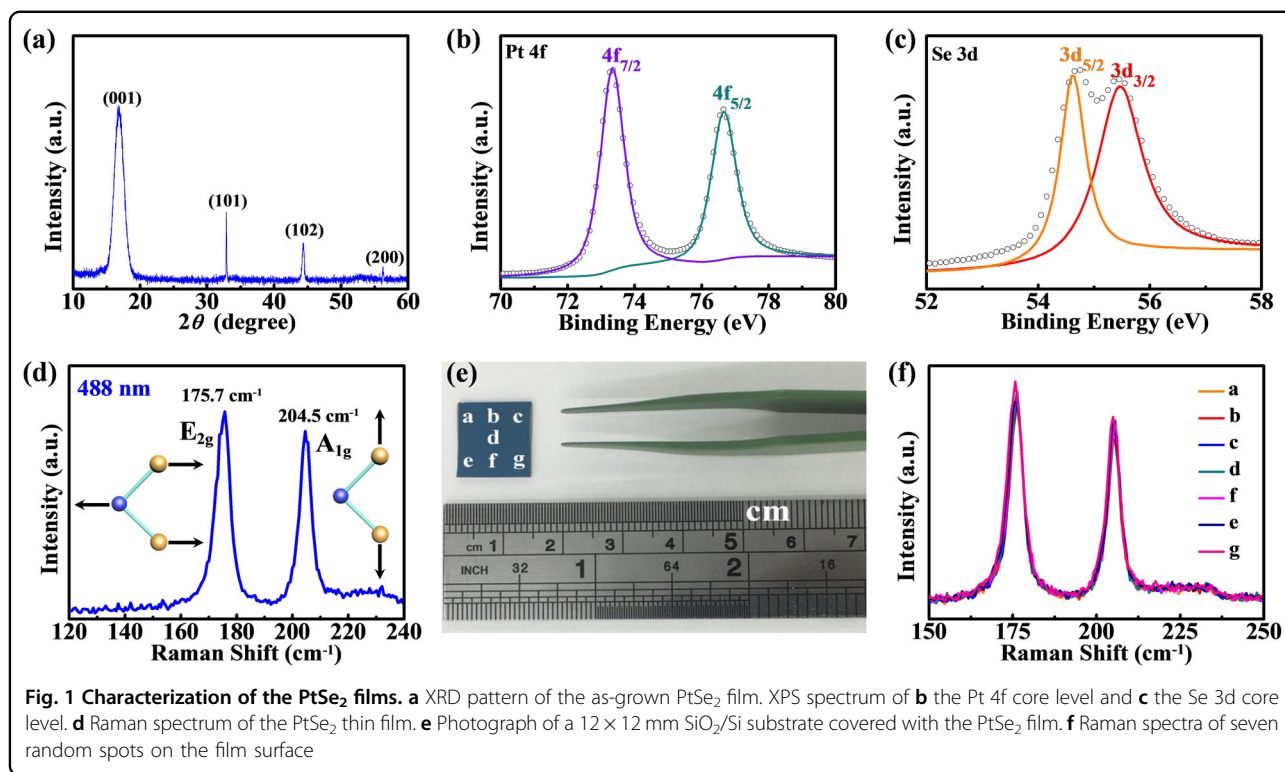
Materials and methods
Preparation and characterization of SiNWA and PtSe₂ films
Vertical SiNWA were prepared on n-Si wafers (resistivity: 1–10 Ω cm) by using a Ag-assisted chemical etching approach[26]. The as-etched SiNWA were dipped in a dilute solution of HNO₃ and HF to dissolve the Ag and Si oxide on the surface. The SiNWA were then cleaned in deionized water. The PtSe₂ film with a vertically standing layered structure was prepared by magnetron sputtering followed by direct selenization (see Supplementary Fig. S1a, b). In brief, a Pt film was deposited on SiO₂/Si using a magnetron sputtering system. The deposition process was carried out at a power of 20 W and a base pressure below 10^{-7} Pa. After magnetron sputtering, the as-prepared Pt film was placed in the center zone of a growth furnace, and elemental selenium (Se) powder was placed at the upstream side. The Se powder was evaporated at 220 °C, and Ar with a flow rate of 50 SCCM (standard cubic cm per min) was used to transport the vaporized Se to the Pt sample. The center temperature of the tube furnace was set to 450 °C and kept stable for 1 h, which was followed by natural cooling to room temperature to complete the annealing process.

Device fabrication and characterization
Poly (methyl methacrylate) (PMMA) as a supporting polymer was spin-coated onto the synthesized PtSe₂ films. The SiO₂ layer under the PtSe₂ was removed by a wet-etching process using a 4 M NaOH solution (Supplementary Fig. S1c). To construct the PtSe₂/SiNWA heterojunction photodetector, a Au (50 nm) top electrode and a Ag (50 nm) bottom electrode were deposited onto the front and back sides of a SiO₂/Si substrate using magnetron sputtering. After being cleaned in deionized water, the PMMA-supported PtSe₂ films were directly transferred onto the top of the SiNWA. After drying at 100 °C for 10 min, the residual PMMA on the PtSe₂ film was removed by acetone (Supplementary Fig. S1d). The absorption spectra of the PtSe₂ film on quartz glass, the SiNWA and the PtSe₂/SiNWA heterojunction were measured by a UV–visible–near-infrared (NIR)

Fig. 1 Characterization of the PtSe₂ films. a XRD pattern of the as-grown PtSe₂ film. XPS spectrum of **b** the Pt 4f core level and **c** the Se 3d core level. **d** Raman spectrum of the PtSe₂ thin film. **e** Photograph of a 12 × 12 mm SiO₂/Si substrate covered with the PtSe₂ film. **f** Raman spectra of seven random spots on the film surface
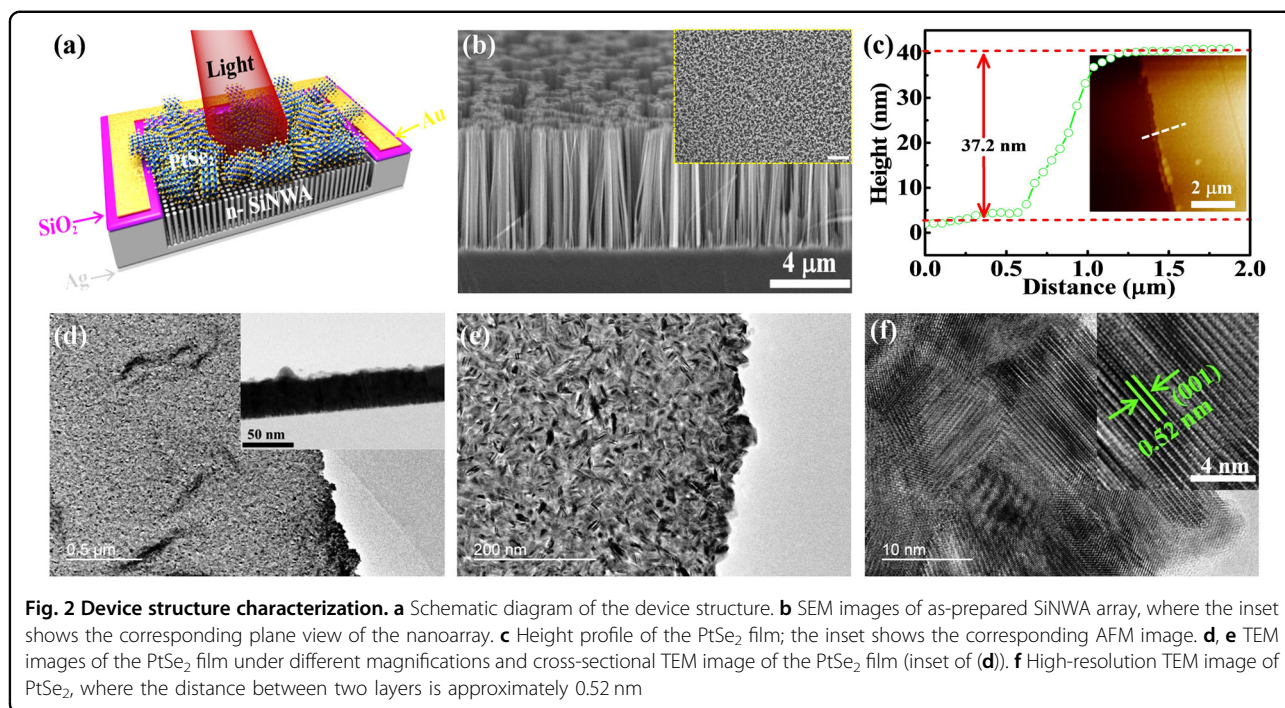
spectrophotometer (UH4150, Hitachi, Japan). Raman spectra measurements were carried out on a HORIBA Raman spectrometer with a 488 nm argon ion laser. The X-ray diffraction (XRD) pattern was recorded using a RigakuSmartLab X-ray diffractometer. The Pt 4f and Se 3d core levels were recorded by X-ray photoemission spectroscopy (XPS), which was performed on a VG ESCALAB 220i-XL analysis system equipped with a monochromatic Al X-ray (1486.6 eV) source. The morphology of the as-prepared SiNWA sample was observed by scanning electron microscopy (SEM, JEOL Model JSM-6490). The morphology, crystal structure and chemical composition of PtSe₂ were investigated using a field emission transmission electron microscope (TEM, JEOL Model JEM-2100F) equipped with an energy-dispersive spectrometer (EDS). The optoelectronic characterization of the devices was performed using a semiconductor parameter analyzer system (Keithley 4200-SCS) at room temperature, and a laser diode (780 nm) was used as the illumination source. To determine the spectral response and time response of the heterojunction devices, a home-built system composed of a light source (LE-SP-LS-XE), a monochromator (LE-SP-M300), an oscilloscope (Tektronix, TDS2012B) and an optical chopper (LE-oc120) was used.

Results and discussion

The crystal structure of PtSe₂ is similar to that of MoS₂ and is composed of one layer of Pt atoms sandwiched

between two layers of Se atoms, as determined from the XRD pattern shown in Fig. 1a. All diffraction peaks at 16.78°, 32.87°, 44.32° and 56.25° can be indexed to the (001), (101), (102) and (200) planes, respectively. XPS characterization was also conducted on the PtSe₂ films. The peaks of the 4f₇/₂ and 4f₅/₂ core levels of Pt are located at 73.35 and 76.65 eV, respectively, and the 3d₅/₂ and 3d₃/₂ core levels of Se are observed at 54.65 and 55.45 eV (Fig. 1b, c)[18]. The typical Raman spectrum of the PtSe₂ film excited by 488 nm light shown in Fig. 1d contains two main peaks at approximately 175.7 and 204.5 cm⁻¹, which are assigned to the E₂g in-plane and A₁g out-of-plane vibration modes, respectively; these results indicate that PtSe₂ has a similar crystal structure as other MX₂ compounds based on comparison with the Raman bands of other MX₂ species[27]. The coverage of the film grown by simple selenization is scalable and controllable even for 2D materials according to previous reports[25]. As shown in Fig. 1e, the SiO₂/Si substrate with a size of approximately 12 × 12 mm was covered uniformly by the PtSe₂ film. To measure the uniformity of the film, seven spots randomly distributed on the film were analyzed by Raman spectroscopy, as shown in Fig. 1f. All spots showed the same two characteristic peaks of PtSe₂ with similar profiles and intensities, revealing the homogeneous growth of PtSe₂ on the wafer with a size of more than a centimeter.

Figure 2a illustrates the device structure of the PtSe₂/SiNWA heterojunction photodetector. The SEM image of

Fig. 2 Device structure characterization. a Schematic diagram of the device structure. **b** SEM images of as-prepared SiNWA array, where the inset shows the corresponding plane view of the nanoarray. **c** Height profile of the PtSe$_2$ film; the inset shows the corresponding AFM image. **d, e** TEM images of the PtSe$_2$ film under different magnifications and cross-sectional TEM image of the PtSe$_2$ film (inset of (**d**)). **f** High-resolution TEM image of PtSe$_2$, where the distance between two layers is approximately 0.52 nm

the SiNWA revealed that the well-aligned SiNWA was approximately 8–10 μm long with a high density and uniformity (Fig. 2b). The atomic force microscopy (AFM) profile across the edge of the PtSe$_2$ nanofilm is shown in Fig. 2c. The thickness of the PtSe$_2$ nanofilm was calculated to be ~37.2 nm, which is fairly consistent with the height acquired from the cross-sectional TEM image of the ordered PtSe$_2$ film (inset of Fig. 2d). The TEM images with different magnifications shown in Fig. 2d, e reveal that the films are composed of highly dense and vertically grown 2D PtSe$_2$ layers with an intermolecular spacing of ~0.52 nm (right inset of Fig. 2f), corresponding to the (001) plane of PtSe$_2$. This unique structure of PtSe$_2$ is probably due to the formation of thick precursor Pt films with a high density, leading to the formation of PtSe$_2$ with a vertical alignment during the selenization process[28]. To further identify the chemical composition of the PtSe$_2$ samples, EDS mapping was conducted, as shown in Supplementary Fig. S2a-c, and confirmed that platinum (Pt) and selenium (Se) were homogeneously distributed over the prepared sample.

Figure 3a depicts the current vs. voltage (*I*–*V*) characteristics of the PtSe$_2$/SiNWA PD in the dark and under light illumination (780 nm, 39.3 mW/cm^2). According to the *I*–*V* curve in the dark, typical rectifying characteristic was observed with a rectification ratio approaching 10^4 at ±5 V, suggesting that a heterojunction was formed between PtSe$_2$ and the SiNWA because the Au and Ag films can provide good Ohmic contact with PtSe$_2$ and the SiNWA, respectively (see Supplementary Fig. S3). By

using the thermionic emission theory-based diode equation (Supporting information), the barrier height of the heterojunction was calculated to be 0.82 eV. Interestingly, the zero bias barrier (Φ_b) of PtSe$_2$/SiNWA, similar to that of the monolayer graphene/Ge Schottky junction[29], dramatically decreased under light illumination, giving rise to an enormous photocurrent under reverse bias, which is consistent with the previous report that light illumination can substantially lower the potential barriers of heterojunctions[30]. The photodetector with the thin PtSe$_2$ film, which was selenized from a 1 nm Pt film, consisted of horizontally aligned nanosheets, as revealed by the TEM images shown in Supplementary Fig. S4a-d. The corresponding thickness of the PtSe$_2$ film was determined to be ~4.3 nm by AFM measurements (Supplementary Fig. S4e). This photodetector also showed similar photoresponse characteristics in the reverse bias region, but its photocurrent was much smaller than that of the thicker PtSe$_2$/SiNWA heterojunction with a vertically aligned layered structure, as shown in Supplementary Fig. S4f. Therefore, we can conclude that the device with a thicker PtSe$_2$ film generated a higher photocurrent, indicating that a substantial amount of carriers was generated in the PtSe$_2$ film[24]. By further investigating the response properties at different voltages, we found that the ON/OFF ratio could be adjusted by the reverse bias. As shown in Fig. 3b, the dark current showed a more significant increase than the photocurrent from 0 to −5 V, and the ON/OFF ratio decreased by two orders of magnitude, reaching
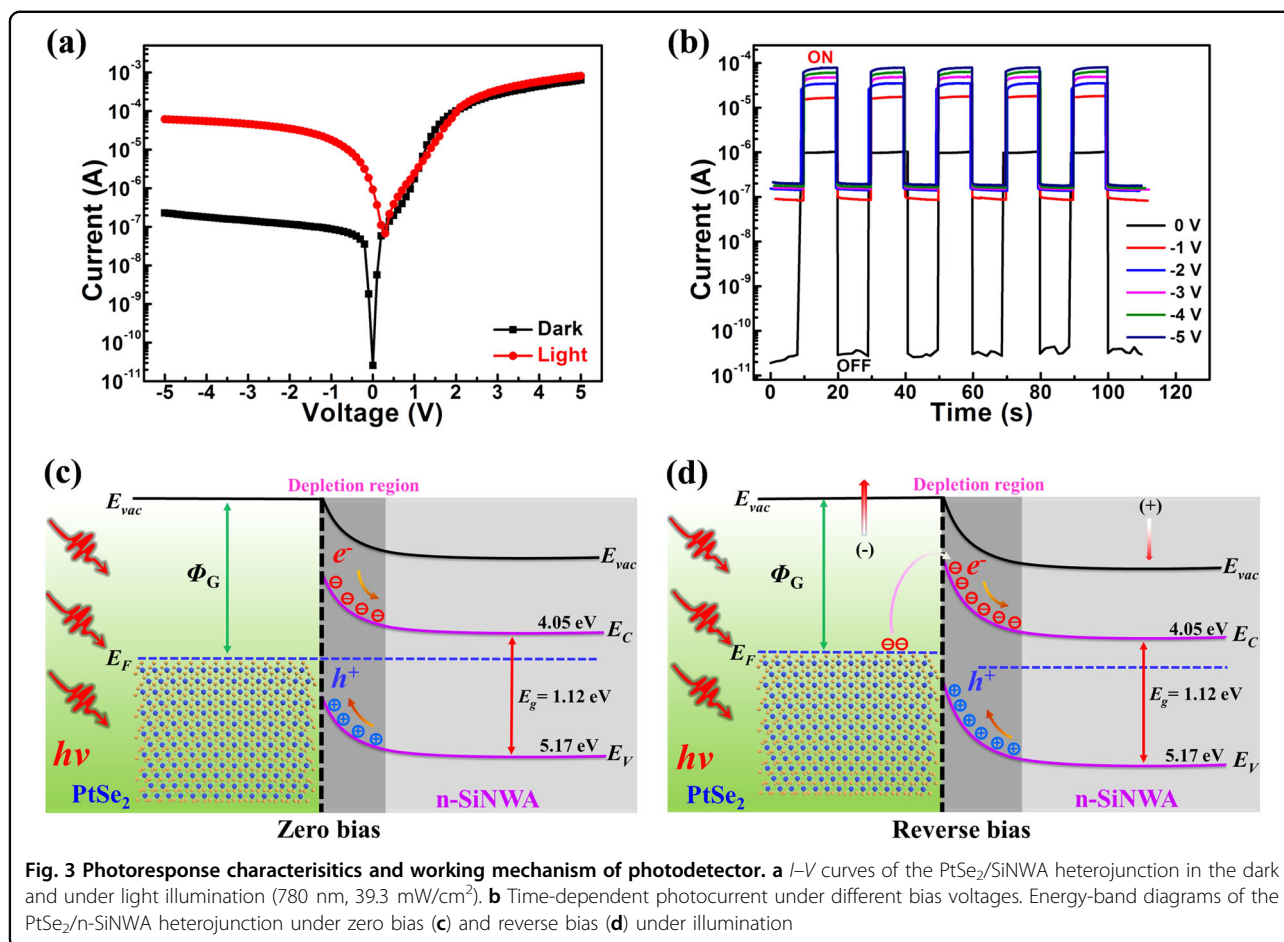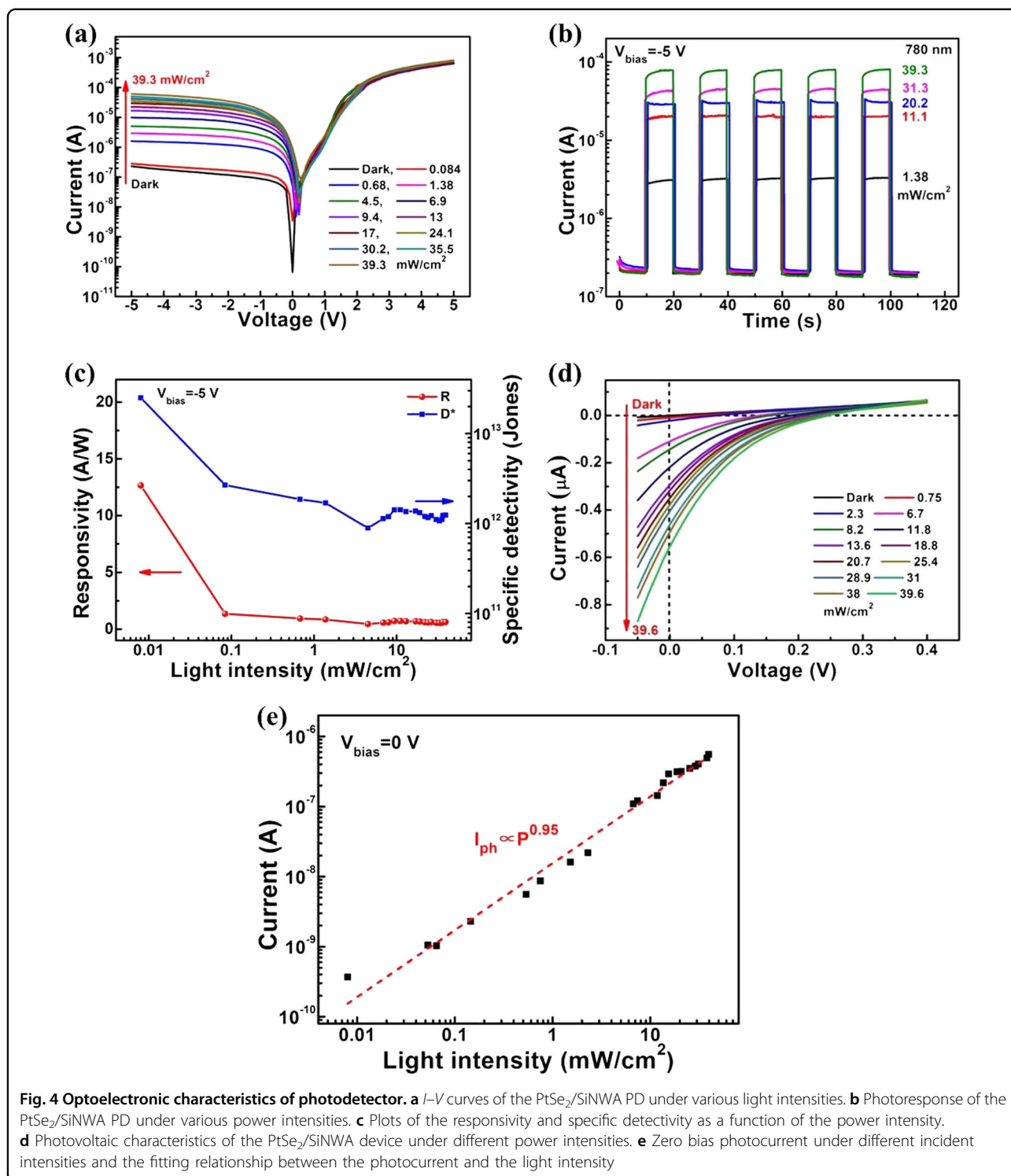
Fig. 3 Photoresponse characterisitics and working mechanism of photodetector. a *I–V* curves of the PtSe$_2$/SiNWA heterojunction in the dark and under light illumination (780 nm, 39.3 mW/cm^2). **b** Time-dependent photocurrent under different bias voltages. Energy-band diagrams of the PtSe$_2$/n-SiNWA heterojunction under zero bias (**c**) and reverse bias (**d**) under illumination

the maximum value (4×10^4) at zero bias. The linear dynamic range (LDR) reached 92 dB under 39.3 mW/cm^2 light illumination at zero bias according to the equation LDR $= 20 \log (I_p/I_d)$; this value is superior to the LDRs of other similar PDs, such as WS$_2$/n-Si (42 dB)[31], InGaAs (66 dB)[32], GaSe/GaSb (77.51 dB)[4], GaS/PET (78.73 dB)[33] and graphene/n-Si (90 dB)[34]. To fully understand the excellent performance of the PtSe$_2$/SiNWA heterojunction, the energy-band diagrams of the heterojunction under zero and reverse bias are shown in Fig. 3c, d. The energy levels of the PtSe$_2$ film were analyzed by ultraviolet photoelectron spectroscopy characterization (see Supplementary Fig. S5), revealing that the Fermi level of the PtSe$_2$ film is located at 5.1 eV[35]. The multilayer 1T-phase PtSe$_2$ film (thickness ≈37.2 nm) could be considered a semimetal[19,36]. Therefore, to achieve an equilibrium state in the dark, electrons would diffuse from the n-SiNWA to PtSe$_2$ due to the difference in Fermi levels between the two materials, which leads to band bending at the n-SiNWA side because of the semi-metallic nature of PtSe$_2$. As a result, a strong built-in electric field is formed in the depletion region, which efficiently separates the photogenerated electron–hole pairs under light illumination, resulting in a sizeable photocurrent. Under reverse bias, an external electric field oriented towards the built-in field increases the separation efficiency of the photogenerated electron–hole pairs. In addition, the reverse bias can also extend the depletion region, allowing more photocarriers to participate in the generation of photocurrent[37].

Quantification of the photodetector response to various light intensities is an important experiment for determining the photodetection performance of a heterojunction[38], so we measured the current vs. bias voltage (log$I$–V) characteristics of the photodetector with respect to different light intensities ranging from the dark to 39.3 mW/cm^2. Clearly, the photocurrent increased with increasing light intensity under reverse bias, resulting in reduced rectifying ratios (Fig. 4a). The reason for the high sensitivity under reverse bias is that photogenerated carriers greatly change the concentration of minority carriers dominating the photocurrent under reverse bias[39]. In addition, the time-dependent photocurrent of the

Fig. 4 Optoelectronic characteristics of photodetector. a *I–V* curves of the PtSe$_2$/SiNWA PD under various light intensities. **b** Photoresponse of the PtSe$_2$/SiNWA PD under various power intensities. **c** Plots of the responsivity and specific detectivity as a function of the power intensity. **d** Photovoltaic characteristics of the PtSe$_2$/SiNWA device under different power intensities. **e** Zero bias photocurrent under different incident intensities and the fitting relationship between the photocurrent and the light intensity

photodetector at −5 V was investigated under light illumination with different power densities of 39.3, 31.3, 20.2, 11.1 and 1.38 mW/cm^2, as shown in Fig. 4b. The photocurrent increased from 1.29 mA/cm^2 to 31.6 mA/cm^2 with the light intensity was tuned from 1.38

to 39.3 mW/cm^2 (illuminated area, $S = 0.0025$ cm^2). To evaluate the performance of the PtSe$_2$/SiNWA heterojunction, the responsivity (R) and specific detectivity (D^*), which are two key parameters, were measured

according to the following equations:

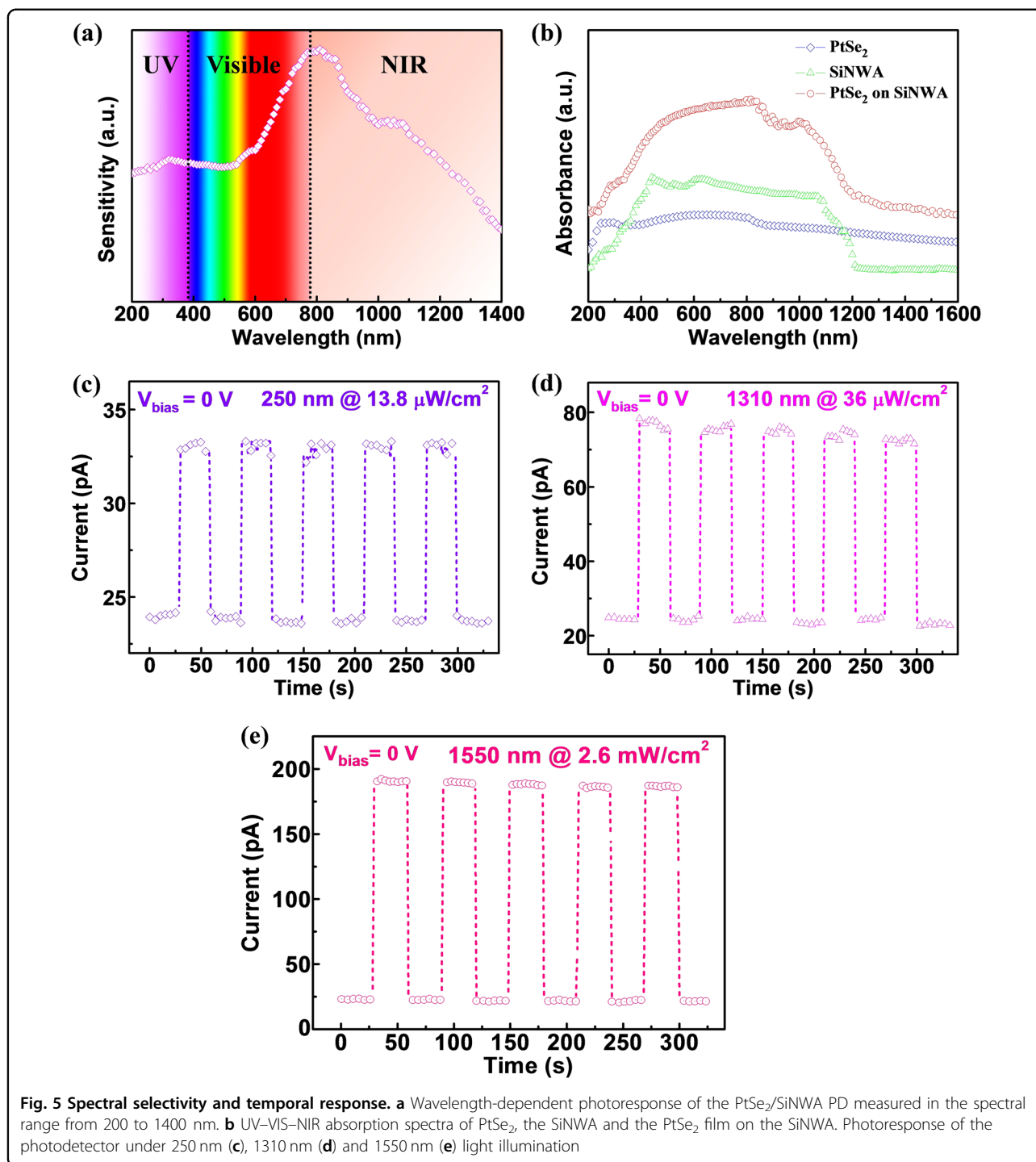$$R = \frac{I_p - I_d}{P_{opt}}, \tag{1}$$

$$D^* = \frac{A^{1/2}R}{(2eI_d)^{1/2}}, \tag{2}$$

where I_p, I_d, P_{opt}, A and e are the photocurrent, dark current, incident light power, effective device area ($A = 0.25\,cm^2$) and absolute value of electron charge (1.6×10^{-19} C). We obtained the largest R and D^* values of 12.65 A/W and 2.5×10^{13} Jones (Jones = cm Hz$^{1/2}$/W), respectively, under a weak light intensity of 0.008 mW/cm^2 at −5 V. These values are comparable to the values reported for WS_2, $MoSe_2$ and MoS_2-based PDs[37,40−42]. Moreover, in Fig. 4c, it is noted that these two metrics decreased with increasing light intensity owing to the increased recombination rate of the photoexcited carriers[43]. Next, the photovoltaic characteristics of the PtSe$_2$/SiNWA heterostructure-based detector were further examined in the dark and under 780 nm light illumination in the light intensity range of 0.75–39.6 mW/cm^2, as shown in Fig. 4d. It is noted that the device exhibits pronounced photovoltaic behavior under light illumination at a zero external bias voltage, indicating that the PtSe$_2$/SiNWA device can function as a self-driven photodetector. With the increase in the power density, the photocurrent increased substantially, as shown in Fig. 4e. The fitting curve of the power law of $I = AP^\theta$ yielded $\theta = 0.95$, which is close to one at zero bias, indicating the presence of low trap states in the PtSe$_2$/SiNWA PD[44].

To assess the broad and sensitive photoresponse performance of the PtSe$_2$/SiNWA photodetector, the spectral response was investigated, as shown in Fig. 5a, which revealed a wide spectral response in the range of 200–1400 nm with the strongest response observed at approximately 800 nm for the PtSe$_2$/SiNWA. As Si-based photodetectors are more sensitive in the range of 300–1100 nm[34], the broad spectral response to light with wavelengths shorter than 300 nm and longer than 1100 nm was due to the strong light absorption of the PtSe$_2$ thin film on the SiNWA according to Fig. 5b. Moreover, the representative response characteristics of the PtSe$_2$/SiNWA PD to deep UV (250 nm) and NIR (1310 and 1550 nm) light were also investigated. Obviously, the device showed a pronounced photoresponse at all these wavelengths. Even though the photoresponse at 250 nm (13.8 μW/cm^2) was not as strong as that at 1310 (36 μW/cm^2) and 1550 nm (2.6 mW/cm^2) due to the lower power density, the photodetector still exhibited an excellent switching stability and reproducibility with an obvious photoresponse, as shown in Fig. 5c. More importantly, Fig. 5d, e shows the

remarkable photoresponse of the photodetector at optical telecommunication wavelengths of 1310 nm (O band) and 1550 nm (C band), respectively, whose photocurrents are smaller than that obtained at 780 nm, which is probably caused by the low photon excitation energy and relatively weak light absorption at long wavelengths (Fig. 5b). However, these response properties have already surpassed those of the conventional Si-based PD, which is insensitive to 1310 and 1550 nm NIR light[45]. The expensive InGaAs-based photodetectors are used in commercially available products for 1550 nm practical detection applications[46]. The high performance of the PtSe$_2$/SiNWA PD with a strong NIR response indicates its good potential for use in optical communication and fiber optic cable testing[47].

Photodetectors are an essential component of some important applications, e.g., optical telecommunication and imaging, for which the response speed of the detector determines the information capacity and frame rate[48−50]. To study the response speed of the fabricated device, an optical signal with varied pulsed frequencies was used, as illustrated in Fig. 6a. As indicted by the schematic diagram of the measurement setup, the temporal photoresponse signal was recorded by a digital oscilloscope as 780 nm light was pulsed at several different frequencies from 1 Hz to 120 kHz by a function generator. Fig. 6b–d show some representative results of the photocurrent produced by the fabricated photodetector under light illumination with frequencies of 1, 10 and 40 kHz. On the other hand, the relative balance $(I_{max} - I_{min})/I_{max}$ of the photocurrent as function of the frequency is depicted in Fig. 6e. It is shown that the relative balance $(I_{max} - I_{min})/I_{max}$ of the photocurrent did not decrease significantly at frequencies as high as 10^4 Hz, indicating that PtSe$_2$/n-SiNWA-based PDs can actually operate at much higher frequencies. Significantly, a 3 dB bandwidth roll-off point occurs at 40 kHz, which was much larger than the small bandwidth of only 50 Hz for the SnS$_2$ nanosheet/PbS CQD hybrid photodetector[5]. In the time domain, the response speed is defined as the total time required for the output to rise from 10 to 90 % of the pulse peak and fall from 90 to 10%. Therefore, by magnifying the shape of the response pulse at 10 kHz, the rise time τ_r and fall time τ_f were measured to be 10.1 and 19.5 μs, respectively (see Fig. 6f). It is worth pointing out that this achieved response speed is much faster than that of other 2D TMD material-based photodetectors[50−52]. We believe that such a fast response speed can be attributed to the strong built-in electric field formed by the PtSe$_2$-SiNWA Schottky junction and the distinct vertically standing layered structure of PtSe$_2$[39]. Furthermore, the long-term stability of a photodetector remains an important concern for the device reliability, so we investigated the air stability of the PtSe$_2$/SiNWA device by repeating the performance test after storing the

Fig. 5 Spectral selectivity and temporal response. a Wavelength-dependent photoresponse of the PtSe$_2$/SiNWA PD measured in the spectral range from 200 to 1400 nm. **b** UV–VIS–NIR absorption spectra of PtSe$_2$, the SiNWA and the PtSe$_2$ film on the SiNWA. Photoresponse of the photodetector under 250 nm (**c**), 1310 nm (**d**) and 1550 nm (**e**) light illumination

device under ambient conditions for a month without any protection. The photodetector showed high durability and almost no change when the device was measured again at 40 kHz (3 dB), and the ultrafast rise/fall time (τ_r/τ_f) of the device was up to 4.1/9.4 μs (see Supplementary Fig. S6), which indicates the high stability of the device under ambient conditions[19].

The main parameters of the PtSe$_2$/SiNWA PD obtained under 780 nm light illumination are shown in Table 1. Notably, the general performance of the present device is much better than that of other 2D material-based photodetectors previously reported, achieving an optimal balance among all the important features. We believe that the excellent device performance can be ascribed to the
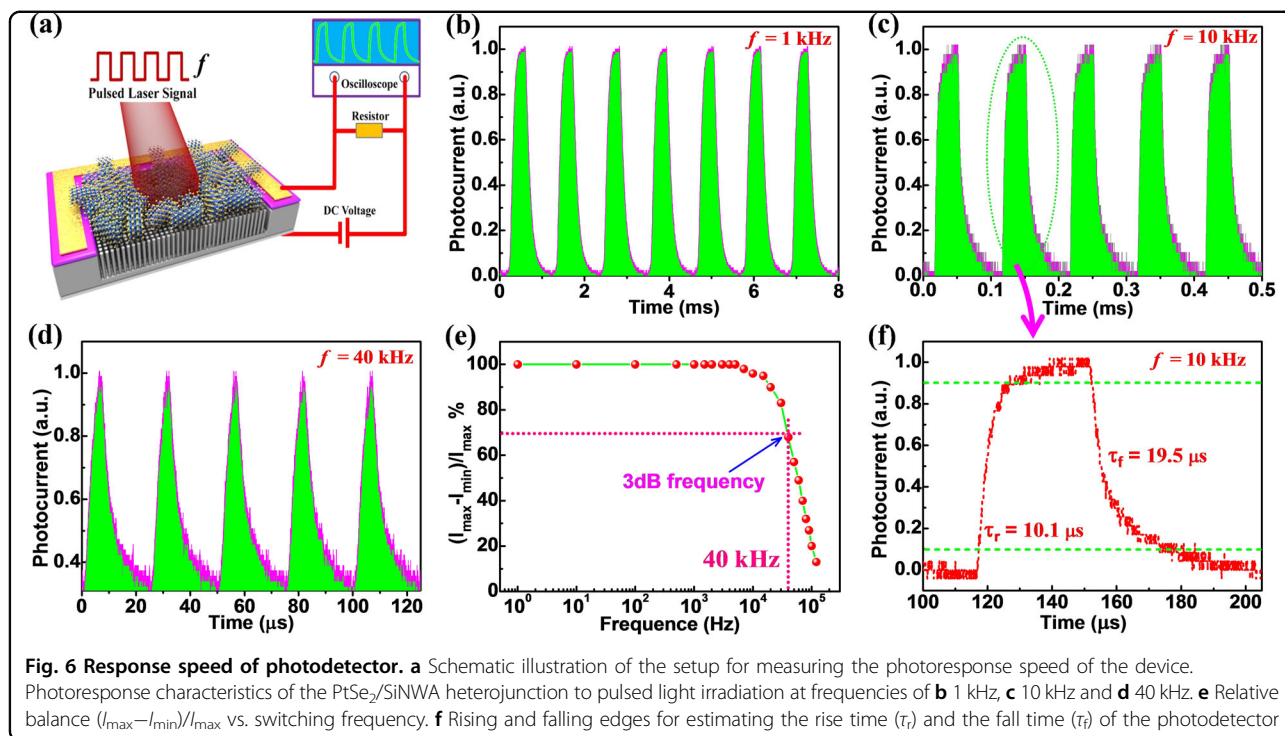
Fig. 6 Response speed of photodetector. a Schematic illustration of the setup for measuring the photoresponse speed of the device. Photoresponse characteristics of the PtSe$_2$/SiNWA heterojunction to pulsed light irradiation at frequencies of **b** 1 kHz, **c** 10 kHz and **d** 40 kHz. **e** Relative balance ($I_{max}-I_{min}$)/I_{max} vs. switching frequency. **f** Rising and falling edges for estimating the rise time (τ_r) and the fall time (τ_f) of the photodetector

Table 1   Performance comparison of our PtSe$_2$/n-SiNWA heterostructure photodetector with that of other 2D material-based photodetectors

Materials and devices	R	τ_r/τ_r	I_{light}/I_{dark}	D* (Jones)	Spectral range (nm)	Ref.
PtSe$_2$/SiNWA heterojunction	12.65 A/W	10.1/19.5 µs	4×10^4	$\sim 10^{13}$	200–1550	This work
GaSe/GaSb heterojunction	115 mA/W	32/24 µs	/	$\sim 10^{12}$	400–1800	[4]
InGaAs/p-Si heterojunction	7.52 A/W	13/16 ms	/	/	400–1250	[6]
MoS$_2$/BP heterojunction	153 mA/W	15/70 µs	/	/	532–1550	[11]
Few-layer BP phototransistor	4.8 mA/W	1 /4 ms	/	/	640–940	[16]
Few-layer PtS$_2$ phototransistor	1560 A/W	4.6/4.6 s	/	$\sim 10^{11}$	/	[17]
Graphene/Ge heterojunction	51.8 mA/W	23/108 µs	$\sim 10^4$	$\sim 10^{10}$	1200–1600	[29]
Graphene/n-Si Schottky junction	0.73 A/W	320/750 µs	$\sim 10^4$	$\sim 10^{12}$	300–1100	[34]
WS$_2$/p-Si heterojunction	5.7 A/W	670/998 µs	$\sim 10^1$	/	340–1100	[37]
Graphene-MoTe$_2$-Graphene heterojunction	110 mA/W	24/46 µs	/	$\sim 10^{10}$	/	[48]
MoS$_2$/n-Si heterojunction	11.9 A/W	30.5/71.6 µs	59.9	$\sim 10^{10}$	300–1100	[50]
MoS$_2$/Graphene heterojunction	835 mA/W	20/30 ms	/	/	420–980	[52]

following factors. (1) The PtSe$_2$ film with a fully vertically standing layered structure greatly facilitated the transport of photoexcited carriers[25,39]. (2) The aligned SiNWA structure strongly suppresses light reflection and enhances light harvesting, which can promote the electron transport efficiency at the interface between the PtSe$_2$ film and the SiNWA[53]. (3) The high-quality heterojunction along with the strong built-in electric field in the depletion layer are beneficial for prolonging the carrier lifetime and shortening the transit time of the photon-generated carriers in the device[54].

Conclusion

In summary, a simple selenization approach was developed for the large-area preparation of a high-quality 2D PtSe$_2$ film with a vertically standing layered structure.

The as-grown $PtSe_2$ film that was integrated with a SiNWA as a high-performance photodetector exhibited a high responsivity of 12.65 A/W at -5 V. Additionally, other key figure-of-merit parameters of the photodetector, such as the detectivity (2.5×10^{13}), rise/fall time (10.1/19.5 µs) and linear dynamic range (92 dB), were all comparable to or better than those of other TMD-based photodetectors. The device showed high air stability over 1 month. Moreover, the $PtSe_2$/SiNWA PD with a broadband photoresponse in the wavelength range from 200 to 1550 nm should have promise for a wide range of applications, including imaging, optical communications and fiber optic cable testing. The large-scale fabrication of $PtSe_2$ thin films could open a myriad of opportunities for fabricating various high-performance integrated optoelectronic devices.

Author details
[1]Department of Applied Physics and Materials Research Center and University Research Facility in Materials Characterization and Device Fabrication, The Hong Kong Polytechnic University, Hung Hom, Kowloon, Hong Kong 99077, China. [2]Department of Physics and Engineering, and Key Laboratory of Material Physics, Zhengzhou University, Zhengzhou, Henan 450052, People's Republic of China. [3]The Hong Kong Polytechnic University Shenzhen Research Institute, Shenzhen, People's Republic of China

Conflict of interest
The authors declare that they have no conflict of interest.

Publisher's note
Springer Nature remains neutral with regard to jurisdictional claims in published maps and institutional affiliations.

Supplementary information is available for this paper at https://doi.org/10.1038/s41427-018-0035-4.

References
1. Hu, X. et al. High-performance flexible broadband photodetector based on organolead halide perovskite. *Adv. Funct. Mater.* **24**, 7373–7380 (2014).
2. Gong, X. et al. High-detectivity polymer photodetectors with spectral response from 300 nm to 1450 nm. *Science* **325**, 1665–1667 (2009).
3. Xie, C., You, P., Liu, Z., Li, L. & Yan, F. Ultrasensitive broadband phototransistors based on perovskite/organic-semiconductor vertical heterojunctions. *Light Sci. Appl.* **6**, e17023 (2017).
4. Wang, P. et al. Arrayed Van Der Waals broadband detectors for dual-band detection. *Adv. Mater.* **29**, 1604439 (2017).
5. Gao, L. et al. Broadband, sensitive and spectrally distinctive SnS_2 nanosheet/PbS colloidal quantum dot hybrid photodetector. *Light Sci. Appl.* **5**, e16126 (2016).
6. Um, D. S. et al. InGaAs nanomembrane/Si van der Waals heterojunction photodiodes with broadband and high photoresponsivity. *ACS Appl. Mater. Interfaces* **8**, 26105–26111 (2016).
7. Tong, X. W. et al. High-performance red-light photodetector based on lead-free bismuth halide perovskite film. *ACS Appl. Mater. Interfaces* **9**, 18977–18985 (2017).
8. An, X., Liu, F., Jung, Y. J. & Kar, S. Tunable graphene-silicon heterojunctions for ultrasensitive photodetection. *Nano Lett.* **13**, 909–916 (2013).
9. Xie, C. et al. Monolayer graphene film/silicon nanowire array Schottky junction solar cells. *Appl. Phys. Lett.* **99**, 133113 (2011).
10. Xie, C. et al. Core-shell heterojunction of silicon nanowire arrays and carbon quantum dots for photovoltaic devices and self-driven photodetectors. *ACS Nano* **8**, 4015–4022 (2014).
11. Ye, L., Li, H., Chen, Z. & Xu, J. Near-infrared photodetector based on MoS_2/black phosphorus heterojunction. *ACS Photonics* **3**, 692–699 (2016).
12. Wu, S. H. et al. High response deep ultraviolet organic photodetector with spectrum peak focused on 280 nm. *Appl. Phys. Lett.* **96**, 093302 (2010).
13. Gity, F. et al. Ge/Si heterojunction photodiodes fabricated by low temperature wafer bonding. *Opt. Express* **21**, 17309–17314 (2013).
14. Xie, C., Mak, C., Tao, X. & Yan, F. Photodetectors based on two-dimensional layered materials beyond graphene. *Adv. Funct. Mater.* **27**, 1603886 (2017).
15. Shi, Y., Li, H. & Li, L. J. Recent advances in controlled synthesis of two-dimensional transition metal dichalcogenides via vapour deposition techniques. *Chem. Soc. Rev.* **44**, 2744–2756 (2015).
16. Buscema, M. et al. Fast and broadband photoresponse of few-layer black phosphorus field-effect transistors. *Nano Lett.* **14**, 3347–3352 (2014).
17. Li, L. et al. Few-layered PtS_2 phototransistor on h-BN with high gain. *Adv. Funct. Mater.* **27**, 1701011 (2017).
18. Wang, Y. et al. Monolayer $PtSe_2$, a new semiconducting transition-metal-dichalcogenide, epitaxially grown by direct selenization of Pt. *Nano Lett.* **15**, 4013–4018 (2015).
19. Zhao, Y. et al. High-electron-mobility and air-stable 2D layered $PtSe_2$ FETs. *Adv. Mater.* **29**, 1604230 (2017).
20. Wang, Z. G., Li, Q., Besenbacher, F. & Dong, M. D. Facile synthesis of single crystal $PtSe_2$ nanosheets for nanoscale electronics. *Adv. Mater.* **28**, 10224–10229 (2016).
21. Lin, X. et al. Intrinsically patterned two-dimensional materials for selective adsorption of molecules and nanoclusters. *Nat. Mater.* **16**, 717–721 (2017).
22. Ali Umar, A., Md Saad, S. K. & Mat Salleh, M. Scalable mesoporous platinum diselenide nanosheet synthesis in water. *ACS Omega* **2**, 3325–3332 (2017).
23. O'Brien, M. et al. Raman characterization of platinum diselenide thin films. *2D Mater.* **3**, 021004 (2016).
24. Yim, C. et al. High-performance hybrid electronic devices from layered $PtSe_2$ films grown at low temperature. *ACS Nano* **10**, 9550–9558 (2016).
25. Wang, L. et al. MoS_2/Si heterojunction with vertically standing layered structure for ultrafast, high-detectivity, self-driven visible-near infrared photodetectors. *Adv. Funct. Mater.* **25**, 2910–2919 (2015).
26. Zhang, X. et al. High-efficiency graphene/Si nanoarray Schottky junction solar cells via surface modification and graphene doping. *J. Mater. Chem. A* **1**, 6593 (2013).
27. Zeng, L. H. et al. High-responsivity UV-Vis photodetector based on transferable WS_2 film deposited by magnetron sputtering. *Sci. Rep.* **6**, 20343 (2016).
28. Jung, Y. et al. Metal seed layer thickness-induced transition from vertical to horizontal growth of MoS_2 and WS_2. *Nano Lett.* **14**, 6842–6849 (2014).
29. Zeng, L. H. et al. Monolayer graphene/germanium Schottky junction as high-performance self-driven infrared light photodetector. *ACS Appl. Mater. Interfaces* **5**, 9362–9366 (2013).
30. Nie, B. et al. Monolayer graphene film on ZnO nanorod array for high-performance Schottky junction ultraviolet photodetectors. *Small* **9**, 2872–2879 (2013).
31. Chowdhury, R. K., Maiti, R., Ghorai, A., Midya, A. & Ray, S. K. Novel silicon compatible p-WS_2 2D/3D heterojunction devices exhibiting broadband photoresponse and superior detectivity. *Nanoscale* **8**, 13429–13436 (2016).
32. Konstantatos, G. et al. Ultrasensitive solution-cast quantum dot photodetectors. *Nature* **442**, 180–183 (2006).
33. Hu, P. et al. Highly responsive ultrathin GaS nanosheet photodetectors on rigid and flexible substrates. *Nano Lett.* **13**, 1649–1654 (2013).
34. Li, X. et al. High detectivity graphene-silicon heterojunction photodetector. *Small* **12**, 595–601 (2016).

35. Park, Y., Choong, V., Gao, Y., Hsieh, B. R. & Tang, C. W. Work function of indium tin oxide transparent conductor measured by photoelectron spectroscopy. *Appl. Phys. Lett.* **68**, 2699–2701 (1996).

36. Lin, S. H. et al. Tunable active edge sites in PtSe$_2$ films towards hydrogen evolution reaction. *Nano Energy* **42**, 26–33 (2017).

37. Lan, C. et al. Zener tunneling and photoresponse of a WS$_2$/Si van der Waals heterojunction. *ACS Appl. Mater. Interfaces* **8**, 18375–18382 (2016).

38. Zhang, Y. et al. Solution assembly MoS$_2$ nanopetals/GaAs n–n homotype heterojunction with ultrafast and low noise photoresponse using graphene as carrier collector. *J. Mater. Chem. C* **5**, 140–148 (2017).

39. Mao, J. et al. Ultrafast, broadband photodetector based on MoSe$_2$/silicon heterojunction with vertically standing layered structure using graphene as transparent electrode. *Adv. Sci.* **3**, 1600018 (2016).

40. Geng, X. et al. Design and construction of ultra-thin MoSe$_2$ nanosheet-based heterojunction for high-speed and low-noise photodetection. *Nano Res.* **9**, 2641–2651 (2016).

41. Choi, W. et al. High-detectivity multilayer MoS$_2$ phototransistors with spectral response from ultraviolet to infrared. *Adv. Mater.* **24**, 5832–5836 (2012).

42. Xue, Y. et al. Scalable production of a few-layer MoS$_2$/WS$_2$ vertical hetero-junction array and its application for photodetectors. *ACS Nano* **10**, 573–580 (2016).

43. Yu, W. et al. Near-infrared photodetectors based on MoTe$_2$/graphene heterostructure with high responsivity and flexibility. *Small* **13**, 1700268 (2017).

44. Xu, H. et al. High responsivity and gate tunable graphene-MoS$_2$ hybrid phototransistor. *Small* **10**, 2300–2306 (2014).

45. Wang, Y., Ding, K., Sun, B., Lee, S.-T. & Jie, J. S. Two-dimensional layered material/silicon heterojunctions for energy and optoelectronic applications. *Nano Res.* **9**, 72–93 (2016).

46. Dou, L. et al. Solution-processed hybrid perovskite photodetectors with high detectivity. *Nat. Commun.* **5**, 5404 (2014).

47. Wang, J. & Lee, S. Ge-photodetectors for Si-based optoelectronic integration. *Sensors* **11**, 696–718 (2011).

48. Zhang, K. et al. Ultrasensitive near-infrared photodetectors based on a graphene-MoTe$_2$-graphene vertical van der Waals heterostructure. *ACS Appl. Mater. Interfaces* **9**, 5392–5398 (2017).

49. Zhang, H. B., Zhang, X. J., Liu, C., Lee, S. T. & Jie, J. S. High-responsivity, high-detectivity, ultrafast topological insulator Bi$_2$Se$_3$/silicon heterostructure broadband photodetectors. *ACS Nano* **10**, 5113–5122 (2016).

50. Zhang, Y. et al. In situ fabrication of vertical multilayered MoS$_2$/Si homotype heterojunction for high-speed visible-near-infrared photodetectors. *Small* **12**, 1062–1071 (2016).

51. Yang, Z. et al. Wafer-scale synthesis of high-quality semiconducting two-dimensional layered InSe with broadband photoresponse. *ACS Nano* **11**, 4225–4236 (2017).

52. Liu, Q. et al. Printable transfer-free and wafer-size MoS$_2$/Graphene van der Waals heterostructures for high-performance photodetection. *ACS Appl. Mater. Interfaces* **9**, 12728–12733 (2017).

53. Luo, L. B. et al. Light trapping and surface plasmon enhanced high-performance NIR photodetector. *Sci. Rep.* **4**, 3914 (2014).

54. Koppens, F. H. et al. Photodetectors based on graphene, other two-dimensional materials and hybrid systems. *Nat. Nanotechnol.* **9**, 780–793 (2014).